We are IntechOpen, the world's leading publisher of Open Access books Built by scientists, for scientists

4,800
Open access books available

122,000
International authors and editors

135M
Downloads

Our authors are among the

154
Countries delivered to

TOP 1%
most cited scientists

12.2%
Contributors from top 500 universities

WEB OF SCIENCE™

Selection of our books indexed in the Book Citation Index in Web of Science™ Core Collection (BKCI)

Interested in publishing with us?
Contact book.department@intechopen.com

Numbers displayed above are based on latest data collected.
For more information visit www.intechopen.com

9

Three Dimensional Capacitive Force Sensor for Tactile Applications

Jose Gerardo Rocha and Senentxu Lanceros-Mendez
University of Minho,
Portugal

1. Introduction

Tactile sensing is one of the most common ways of interacting with the environment. So common that it is most of the time unnoticed unless unpleasant sensations are involved (e.g. burning). The human being is completely covered, though the skin, by tactile sensors providing information about pressure and temperature variations translated into pleasant or unpleasant sensations, warnings messages and so on.

The tactile resolution of the human skin can be as precise as tenths of millimeters in the fingertips up to some centimeters in other parts of the body.

One interesting issue of the tactile sensing of the human skin is that it is not only responsive to normal forces, but also to shear, which is particularly important by graving delicate object and sensing roughness, among others. We refer two examples:

- People with serious motor limitations have, in most of the cases, a decrease of sensitivity in the areas of the body in contact with the supporting surfaces (e.g. beds or wheel chairs). Their limited motor capacity does not allow them to regularly change position autonomously, as a healthy person would do unconsciously. Consequently, insufficient sanguineous irrigation occurs as a result of pressure exceeding the tissue capillary pressure for a long time, depriving tissues of oxygen and essential nutrients, leading to ischemia and hypoxia, which then causes the development of pressure ulcers. These ulcers can be developed either due to a constant pressure exerted normally to the skin or due to a shear pressure also in the skin. One way to reduce the probability of pressure related ulcer formation is to monitor the three axes force that people with serious motor limitations exert on the supporting surfaces. In order to do that, an array of three axes force sensors must be placed along a bed sheet, for example.
- Gripping and manipulation of objects by robots require robust and reliable feedback of forces. For example, when a manipulator holds a fragile object, on the one hand, the force normal to the object must be as low as possible, and on the other hand, with a low normal force, the falling risk increases. One solution consists in measuring the shear forces and appropriately feedback them to electronics in order to adjust the necessary normal force. In order to do this a three axis soft flexible force sensor system seems to be more appropriate for delicate objects.

A great challenge in the development of artifacts such as robot fingers and portable terminals is to create tactile information processing systems that closely resemble those of humans, both in terms of flexibility, durability and versatility. Such artifacts will allow

Source: Sensors, Focus on Tactile, Force and Stress Sensors, Book edited by: Jose Gerardo Rocha and Senentxu Lanceros-Mendez,
ISBN 978-953-7619-31-2, pp. 444, December 2008, I-Tech, Vienna, Austria

application areas for tactile sensors such as food processing, bio-medical, entertainment, future domestic and service industries and robotics in medicine for minimally invasive and micro-surgeries.
A major requirement of a tactile sensor is to have the ability of measuring the magnitude and location of an exerted force over the sensor. Further, well-designed tactile sensors must be thin and flexible, similarly to sensitive skin.
Further, capacitive sensors are used in a wide variety of measurement and control systems, such as liquid-level gauges, pressure meters, accelerometers, precision positioners, and as described in this chapter, as force sensors. In these applications, the capacitances to be measured often range from tenths to tens of picofarads. In particular, there are a large variety of applications for capacitive sensors acting as three axis force sensors.
This chapter is organized as follows: Section 2 describes different types of tactile sensors, giving examples of the ones using electromagnetic, piezoelectric, resistive and piezoresistive working principles. In section 3, a complete description of a three dimensional tactile sensor based on capacitive elements is performed. Section 4 describes some readout electronic techniques that could be applied to the sensor of section 3, namely switched-capacitor, capacitance to pulse-width, capacitance to duty-cycle and capacitance to frequency techniques. Section 5 is devoted to a complete description of a capacitance to voltage conversion technique that shows very good results when associated to the sensor of section 3. Finally, section 6 is dedicated to the conclusions.

2. Overview about tactile sensors

According to their working principle, the tactile sensors can be classified as electromagnetic, piezoelectric, resistive, piezoresistive, capacitive, etc. In the following subsections and in section 3, some examples of sensors based on some of these principles are described.

2.1 Electromagnetic tactile sensors

Among all types of tactile sensors using the electromagnetic principle, the fiber Bragg grating sensors (FBG) are the ones showing very promising results.
FBG sensors are fabricated by taking a given length of a single mode optical fiber, subjecting it to high pressure hydrogenation to increase its photosensivity, and then focusing an intense interference pattern of ultra violet light onto the core of the fiber using a laser and tipically a phase mask [1]. The grating consists on an axially periodically varying refractive index along the core of the fiber. The effect of the grating is to convert the fiber into a high wavelength-selective mirror. If broadband light is directed through the fiber, a narrow band of light will be reflected. Its center, or Bragg wavelength, is given by:

$$\lambda_B = 2n\Lambda. \tag{1}$$

where n is the effective refractive index of the fiber core mode and Λ is the period of the grating. When the fiber is subjected to an increase in strain or temperature, both n and Λ are affected and the Bragg wavelength increases [2].
Sensor systems involving such gratings typically work by injecting light from a spectrally broadband source into the fiber, with the result that the grating reflects a narrow spectral component at the Bragg wavelength or, in transmission mode, with this component missing from the observed spectrum. Fig. 1 illustrates this process [3].

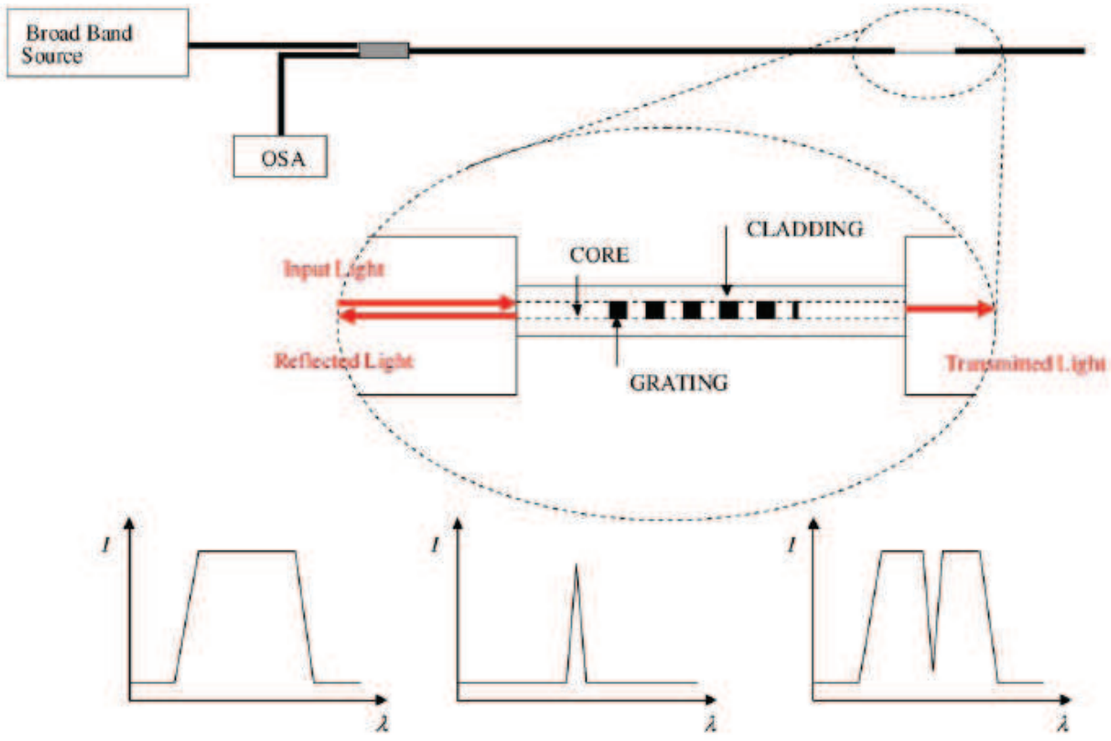

Fig. 1. Fiber Bragg Grating sensor encoding operation [3].

2.2 Piezoelectric tactile sensors

Piezoelectric tactile sensors are based on materials that show the piezoelectric effect, that is, when a pressure change is applied to them, it is possible to measure an electrical potential difference between their surfaces. As the potential difference is proportional to the variation of pressure instead to the pressure itself, some techniques are necessary to build piezoelectric tactile sensors. Tanaka et. al., presented a sensor system based on a PVDF piezoelectric polymer film and a soft rubber [4]. The surface of the sensor is heated through a temperature controller mechanism. The sensor is attached on the tip of a robot finger and the base of the finger is mounted on a linear slider. Using this sensor system, the active sensing was designed resembling human motions for tactile perception in mind. Two kinds of active sensing were introduced to obtain the information on feelings of vibration and warmth, as follows:

- For obtaining the information on warmth, the sensor is moved and contacted with the object through the trajectory control of the contact pressure.
- For obtaining the information on feelings of vibration, the sensor is slid over the object at a constant speed.

The geometry of the sensor is shown in Fig. 2. The sensor is attached on the tip of a robot finger. The base of the sensor is composed by an acrylic block and a vulcanized rubber. Around the base, a copper tape overlaid with Nichrome wire, a PVDF film, and a protective layer of acetate film are stacked in sequence. A thermistor is attached on the side of the sensor. The Nichrome wire and the thermistor are used for heating the sensor and measuring the sensor's temperature, respectively. The robot finger is composed by a piezoelectric bimorph strip and an aluminum beam. The piezoelectric bimorph strip is used

to press the sensor on an object. A strain gauge is attached on the base of the aluminum beam for the measurement of the contact force applied by the finger.

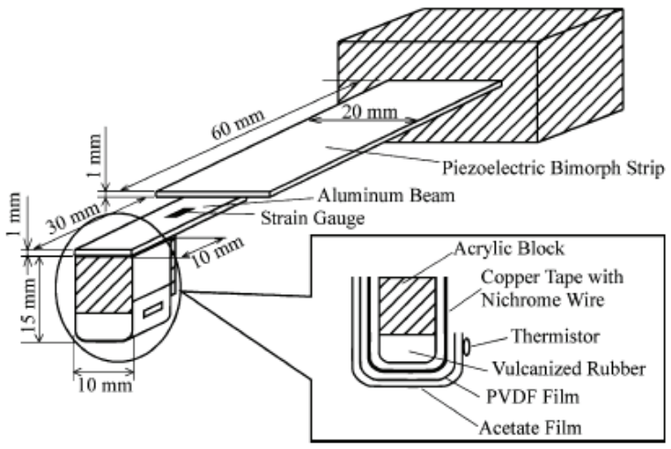

Fig. 2. Geometry of a piezoelectric tactile sensor. The sensor is attached on the tip of the robot finger driven by the piezoelectric bimorph strip. The sensory receptor is the PVDF film[4].

Fig. 3 shows the schematic illustration of the sensing process.

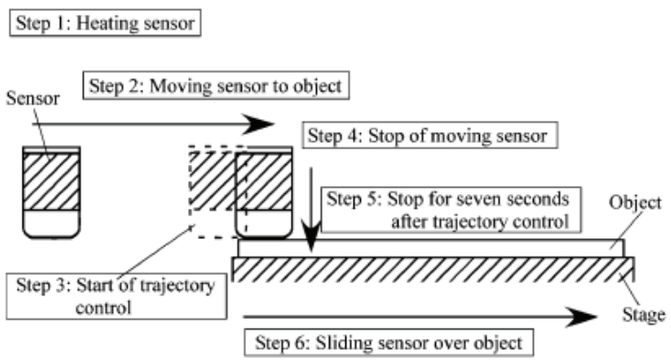

Fig. 3. Schematic illustration of sensing process. Two kinds of active sensing are introduced. First, the sensor is heated. After the sensor's temperature is constant, the experiment through contact is performed (steps 2to 5) in order to obtain the information on warmth. Then, the experiment through slide is performed (step 6) in order to obtain the information on feelings of vibration [4].

First, the sensor is heated until its temperature is constant. Then, the experiment through contact is performed (steps 2 to 5) in order to obtain the information on warmth. Then, the experiment through slide is performed (step 6) in order to obtain the information on feelings of vibration

Another technique that employs piezoelectric elements for tactile sensing is the one based on resonant vibrating sensors [5, 6]. The principle of the piezoelectric vibration-type sensor can be explained with the help of Fig. 4 [6]. This sensor has two electrodes: one for driving

and the other for measuring. The driving electrode is supplied with an alternating current, and the sensor resonates due to the inverse piezoelectric effect. Due to this, a voltage is generated by the piezoelectric effect in the measuring electrode. An external force applied to the sensor causes a change in the mechanical impedance between the piezoelectric elements. This change can be measured at the measuring electrode.

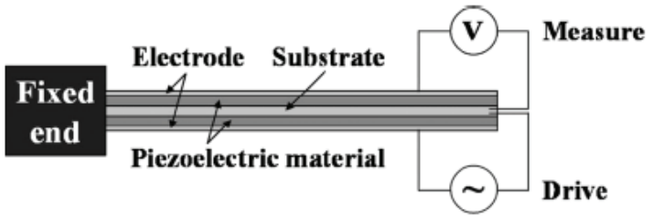

Fig. 4. Piezoelectric vibration-type sensor. The system is composed by a substrate, piezoelectric materials, and electrodes [6].

2.3 Resistive tactile sensors

Resistive tactile sensors usually use strain gauge as sensing elements. Hwang et. al. describe an approach that uses the deformation of a polymer substrate where the strain gauge elements are fabricated. Fig. 5 shows a schematic view of the proposed tactile sensor. The strain sensitive elements, i.e., the strain gauges, were embedded into a ductile polymer substrate. A thin film of metal is used for fabricating the strain gauges. Both the polymer and the thin film allow the sensor to be flexible. A bump structure is placed on top of the sensor surface to facilitate load distribution. When an external force is applied to the device, the thin film structure and the polymer suffers a deformation that induces strain and therefore changes in the electrical resistance of the strain gauge [7].

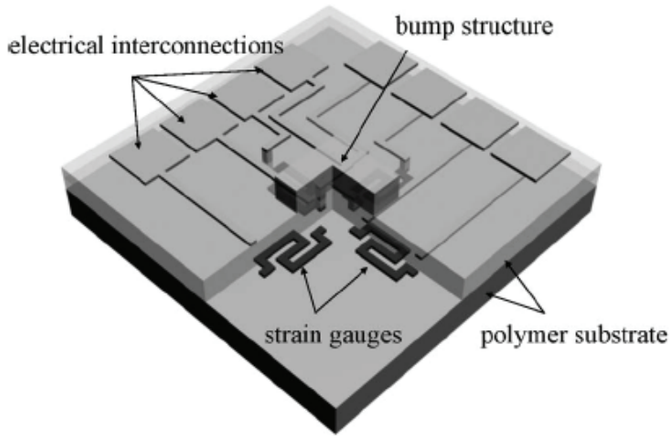

Fig. 5. Schematic view of the proposed tactile sensor. The strain-sensitive elements, i.e., the strain gauges, are embedded in a ductile polymer substrate that is used to measure the strains in the polymer substrate. A bump structure, used for load distribution, is placed on top of the sensor surface [7].

The normal and shear load sensing principles of the proposed sensor are shown in Fig. 6. Strain gauges are embedded at the center of a ductile polymer substrate. When a normal

load is applied on the surface of the sensor, the substrate deforms. This deformation induces equal strains on both strain gauges, as shown in Fig. 6(a). When a shear load is applied, as shown in Fig. 6(b), one strain gauge experiences tensile strains, while the other experiences compressive strains. This difference results in different measurable voltage drops across each strain gauge, which allows the shear load to be determined. An unknown load can be found by superposition of these two cases. From these sensing principles, the tactile-sensor unit cell consists of four strain gauges for shear load detection in the x- and y-directions.

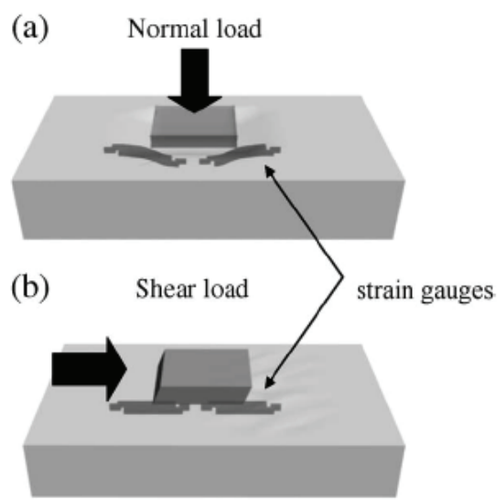

Fig. 6. Normal and shear load sensing principles. (a) In the case of a normal load, both strain gauges are subjected to tensile stress. (b) In the case of a shear load, one strain gauge is subjected to tensile stress, and the other is subjected to compressive stress[7].

2.4 Piezoresistive tactile sensors

The piezoresistive tactile sensors are based on piezoresistive elements, that is, elements based on materials that show changes in their electrical resistance proportional to the applied pressure. Contrarily to the piezoelectric elements, these ones can act as tactile sensors even in the presence of static pressures. The material most effectively used to build piezoresistive elements is silicon. As this material is also the basis of the microelectronic circuits, it is a common procedure to place the sensors as well as the readout electronics into the same device [8].

Balke et. al. [9] presented a sensor system consisting on a cantilever structure with integrated probing tip with variable heights and shapes. The signal of the deflection is processed by a piezoresistive Wheatstone bridge configuration into an electrical signal.

The sensor is fabricated in a standard silicon micromachining process (Fig. 7). The process started with {100}-n-silicon wafer with a thickness of 350 µm. The wafer was scratched and broken into samples of 26 x 26 mm^2. The basic steps are lithography with a positive S1818-photoresist, oxidation of the samples at 1100^oC, wet chemical etching in aquaeous potassium hydroxide and tetramethylammonium hydroxide solutions and boron diffusion. Some of the standard processes can be modified or substituted by other processes.

There are however piezoresistive tactile sensors that do not use silicon. Wisitsoraat et. al. present a tactile sensor using indium tin oxide (ITO) as piezoresistive element [10]. The MEMS tactile sensor structure (Fig. 8) consists of a multi-layer AlN/Al/Cr square shuttle

plate (200 µm× 200 µm) with four arms on which four piezoresistors of ITO are placed. In addition, contacts of each piezoresistor are coated with Cr/Au. When an external force is applied, the piezoresistors changes electrical resistance due to induced strain. The gold layer is used as the electrode and bonding pad of the piezoresistor. The AlN layer acts as an insulator providing isolation between the Cr/Al membrane and the piezoresistor. The Cr layer is used as an adhesive film and the thick Al layer is used to increase the flexibility and robustness of the membrane structure.

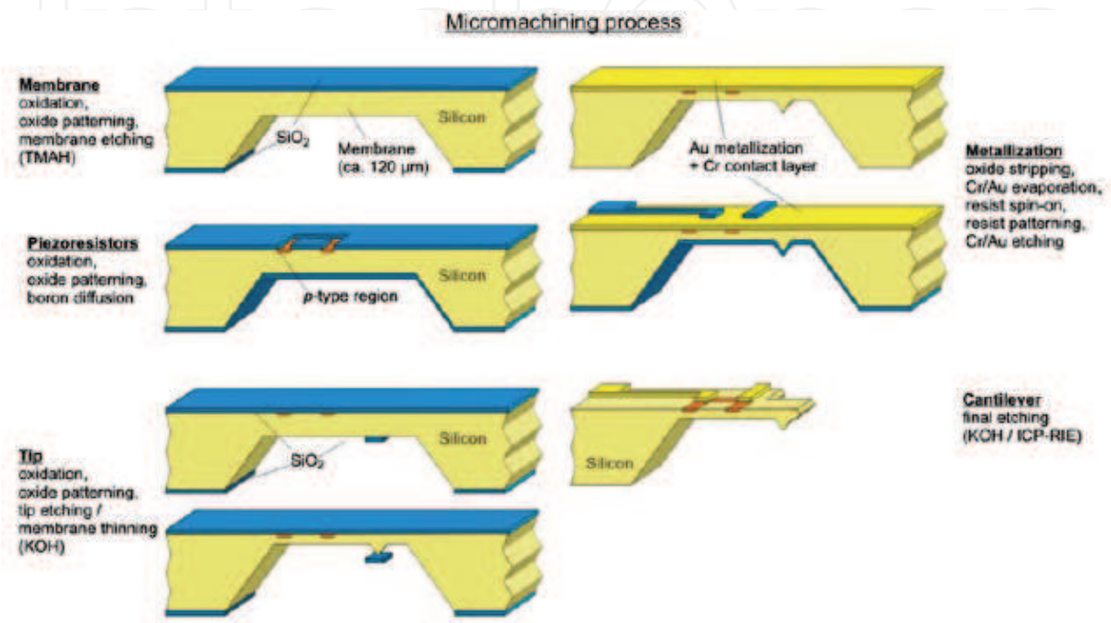

Fig. 7. Representation of the five main stages of a standard silicon micromachining process for the fabrication of the piezoresistive tactile sensor [9].

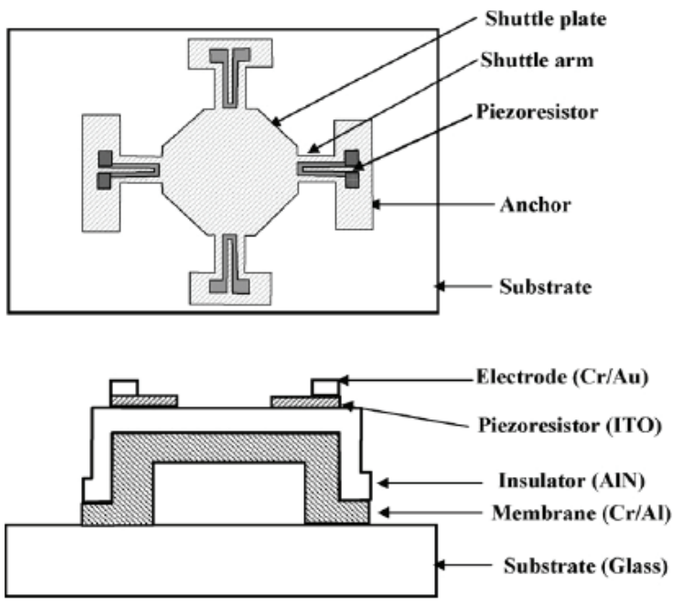

Fig. 8. Structure of a ITO-based piezoresistive tactile sensor [10].

3. Theoretical description of a three dimensional capacitive force sensor

Among the capacitive tactile sensors, it is possible to find recent articles describing epoxy-based [11] or foam-based [12] ones. In the following a general a three dimensional, 3D, capacitive tactile sensor based on a flexible dielectrics will be described in detail.

Fig. 9 shows a schematic diagram of the sensor. It consists on a flexible dielectric material such as rubber or foam in which a square of conductive material (such as aluminum) is placed at its top and four squares of conductive material are placed at its bottom. The thickness of the dielectric material is *t*, the dimension of the conductive square side is *D* and the distance between the two conductive squares of the bottom is *d*. The conductive material can be deposited by different methods, such as thermal evaporation, physical vapor depositions, etc, depending on the dielectric used and the dimensions of the capacitors.

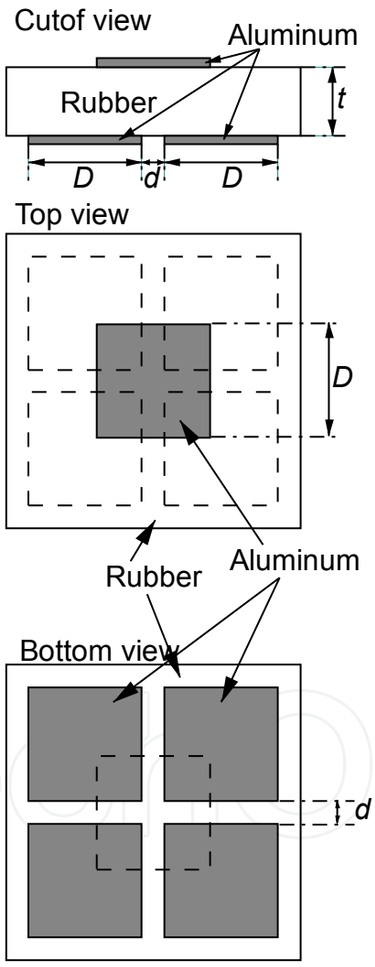

Fig. 9. Schematic diagram of the force sensor consisting on a flexible dielectric material (e.g. rubber) in which a square of aluminum is placed at its top and four squares of aluminum are placed at the bottom.

The arrangement forms four capacitors, C_1, C_2, C_3 and C_4, as shown in Fig. 10. In the following sections, the *x*, *y* and *z* displacement values are calculated for forces applied along the *xx*, *yy* and *zz* axes either independently or simultaneously.

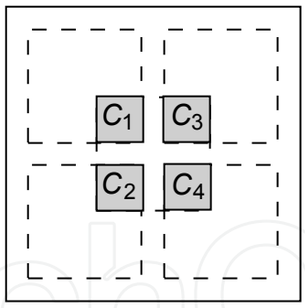

Fig. 10. Representation of the four capacitors formed by the conductive material arrangement.

3.1 Sensor with no applied pressure

At the steady state and with no applied pressure, the capacitance of the capacitors is given by:

$$C_1 = C_2 = C_3 = C_4 = \frac{\varepsilon_r A}{t}, \tag{2}$$

where ε_r is the dielectric constant of the flexible dielectric material and A is the area of the parallel plate capacitor, given by:

$$A = \left(\frac{D-d}{2}\right)^2. \tag{3}$$

Therefore, the capacitances are given by:

$$C_1 = C_2 = C_3 = C_4 = \frac{\varepsilon_r \left(D-d\right)^2}{4t}, \tag{4}$$

3.2 Sensor with a pressure applied along the zz axis

The sensor with a force applied in the *zz* axis is represented in Fig. 11.

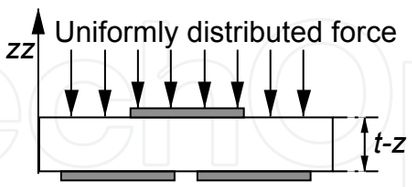

Fig. 11. Sensor with a force applied along the zz axis.

In this case, the values of the capacitances are given by:

$$C_1 = C_2 = C_3 = C_4 = \frac{\varepsilon_r \left(D-d\right)^2}{4\left(t-z\right)}, \tag{5}$$

where z is the displacement along the *zz* axis. The minus sign in front of z is due to the fact that the applied pressure will decrease the thickness of the dielectric. Therefore, the displacement, z, along the *zz* axis can be calculated by solving equation 5 in order to z:

$$
\begin{aligned}
z &= -\frac{(d-D)^2 \varepsilon_r}{4C_1} + t \\
&= -\frac{(d-D)^2 \varepsilon_r}{4C_2} + t \\
&= -\frac{(d-D)^2 \varepsilon_r}{4C_3} + t \\
&= -\frac{(d-D)^2 \varepsilon_r}{4C_4} + t
\end{aligned} \tag{6}
$$

Equation 6 shows four different forms to calculate the z displacement value. The final value is obtained through a simple average procedure, reducing the resultant error.

3.3 Sensor with a pressure applied along the xx axis or the yy axis

The force sensor with a pressure applied along the *xx* axis is shown in Fig. 12.

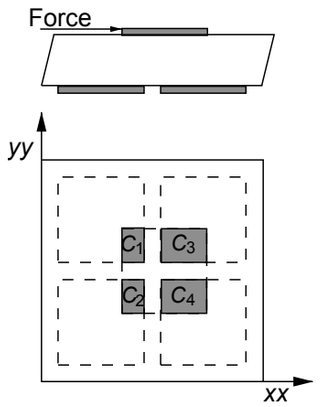

Fig. 4. Force sensor with a pressure applied along the xx axis.

In this case, the values of the capacitances are given by:

$$
\begin{aligned}
C_1 = C_2 &= \frac{\varepsilon_r (d-D)(d-D+2x)}{4t} \\
C_3 = C_4 &= \frac{\varepsilon_r (d-D)(d-D-2x)}{4t}
\end{aligned} \tag{7}
$$

where x is the displacement of the conductive square of the top along the *xx* axis. Solving equation 7 in order to x, it is obtained:

$$
\begin{aligned}
x &= \frac{1}{2}\left(-d + D + \frac{4C_1 t}{\varepsilon_r (d-D)}\right) \\
&= \frac{1}{2}\left(-d + D + \frac{4C_2 t}{\varepsilon_r (d-D)}\right) \\
&= \frac{1}{2}\left(-d - D - \frac{4C_3 t}{\varepsilon_r (d-D)}\right) \\
&= \frac{1}{2}\left(-d - D - \frac{4C_4 t}{\varepsilon_r (d-D)}\right)
\end{aligned} \tag{8}
$$

In a similar way, the values of the capacitances expressing a displacement *y* along the *yy* axis are given by:

$$C_1 = C_3 = \frac{\varepsilon_r (d-D)(d-D+2y)}{4t}$$
$$C_2 = C_4 = \frac{\varepsilon_r (d-D)(d-D-2y)}{4t} \tag{9}$$

In this case, the value of *y* can be obtained from:

$$y = \frac{1}{2}\left(d - D - \frac{4C_1 t}{\varepsilon_r (d-D)} \right)$$
$$= \frac{1}{2}\left(-d + D + \frac{4C_2 t}{\varepsilon_r (d-D)} \right)$$
$$= \frac{1}{2}\left(d - D - \frac{4C_3 t}{\varepsilon_r (d-D)} \right) \tag{10}$$
$$= \frac{1}{2}\left(-d + D + \frac{4C_4 t}{\varepsilon_r (d-D)} \right)$$

Both in the *x* and *y* displacements, the thickness of the dielectric, *t*, decreases, so in precision applications, this change must be taken into account. The calculation can be performed as follows: considering Fig. 13, the horizontal displacement *hd* is given by:

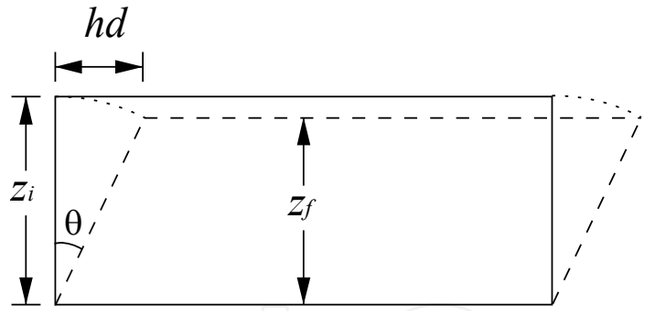

Fig. 13. Decrease of the thickness of the dielectric caused by forces applied horizontally.

$$hd = \sqrt{x^2 + y^2} \tag{11}$$

The angle θ can be calculated from the horizontal displacement:

$$\theta = \arcsin \frac{hd}{z_i} \tag{12}$$

where z_i is the initial value of *z*. Finally, the final value of *z* (z_f) is given by:

$$z_f = z_i \cos\theta \tag{13}$$

In the more general case of forces applied along the 3 axes a specific formalism, described below (section 3.4), must be taken into account.

3.4 Sensor with a pressure applied along the three axes

In the case of pressures applied along the three axes, the conductive material on the top of the sensor will be moved along the *xx*, *yy* and *zz* axes, and the values of the capacitances are:

$$\begin{aligned} C_1 &= \frac{\varepsilon_r (d-D+2x)(d-D-2y)}{4(t-z)} \\ C_2 &= \frac{\varepsilon_r (d-D+2x)(d-D+2y)}{4(t-z)} \\ C_3 &= \frac{\varepsilon_r (d-D-2x)(d-D-2y)}{4(t-z)} \\ C_4 &= \frac{\varepsilon_r (d-D-2x)(d-D+2y)}{4t} \end{aligned} \tag{14}$$

In this case, four equations and three unknowns are obtained, meaning that there are several solutions for the unknowns. The values of the *x*, *y* and *z* displacements are:

$$\begin{aligned} x &= \frac{(C_1-C_3)(d-D)}{2(C_1+C_3)} \\ &= \frac{(C_2-C_4)(d-D)}{2(C_2+C_4)} \end{aligned} \tag{15}$$

$$\begin{aligned} y &= \frac{(C_1-C_2)(d-D)}{2(C_1+C_2)} \\ &= \frac{(C_3-C_4)(d-D)}{2(C_3+C_4)} \end{aligned} \tag{16}$$

$$\begin{aligned} z &= -\frac{\varepsilon_r C_1 (d-D)^2}{(C_1+C_2)(C_1+C_3)} + t \\ &= -\frac{\varepsilon_r C_2 (d-D)^2}{(C_1+C_2)(C_2+C_4)} + t \\ &= -\frac{\varepsilon_r C_3 (d-D)^2}{(C_1+C_3)(C_3+C_4)} + t \\ &= -\frac{\varepsilon_r C_4 (d-D)^2}{(C_2+C_4)(C_3+C_4)} + t \end{aligned} \tag{17}$$

In this case, there are two different forms to calculate the *x* and *y* displacements and four different forms to calculate the *z* value. The final value of each displacement can be obtained through a simple average procedure, reducing the resultant errors, as described for the previous cases.

Finally, the applied force along the three axes can be calculated by multiplying the displacement by the elasticity constant of the dielectric medium.

4. Overview about readout electronic circuits for capacitive sensors

Regarding readout circuits for capacitive sensors, there are several configurations that can be used and are found in literature, such as:

- switched-capacitor capacitance to voltage converter [13, 14],
- capacitance to pulse-width modulator [1, 16],
- capacitance to duty-cycle converter [17],
- capacitance to frequency converter [18] and complete signal processing units [19].

4.1 Switched-capacitor capacitance to voltage converter

The first circuit for capacitance measurements described here is a switched-capacitor capacitance to voltage converter, which can be applied to differential capacitive sensors. The functional block schematic of the proposed signal conditioner is shown in Fig. 14.

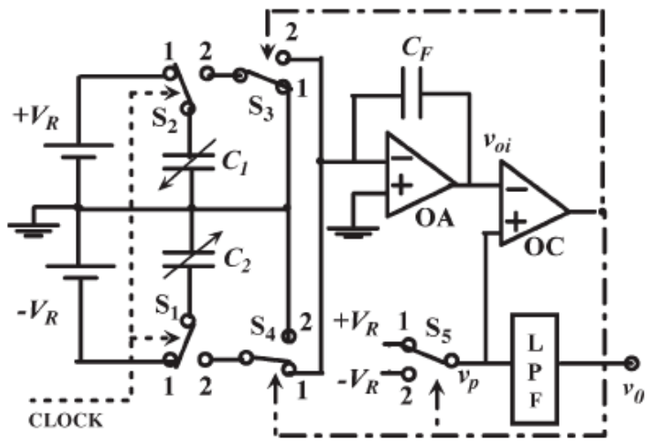

Fig. 14. Block diagram of the switched-capacitor signal-conditioning circuit [14].

Switches S_1, S_2, S_3, S_4, and S_5 are all single-pole double-throw analog switches. Switches S_1 and S_2 are controlled by a high-frequency clock having 50% duty-cycle and switch the capacitances C_1 and C_2 of the sensor between the charge and discharge positions. Switches S_3 and S_4 are connected such that only one of the capacitors (C_1 or C_2) charges the feedback capacitance C_F at a given time. The circuit is essentially a relaxation oscillator with the operational amplifier (OA) working as a switched capacitor integrator, while switch S_5, in conjunction with comparator OC, provides the necessary hysteresis and positive feedback required for oscillation [14].

Let us assume that initially, the integrator output is positive and increasing. The comparator output is high, and hence, switches S_3, S_4, and S_5 will be at position 1. S_1 and S_2 will toggle between positions 1 and 2 for every clock cycle. When S_1 and S_2 are in position 1, the C_1 voltage will be $+V_R$, and the C_2 voltage will be $-V_R$. When the clock becomes low, switches S_1 and S_2 will go to position 2, and the charge in the capacitor C_2 will be transferred to the integrator capacitor C_F, while the charge in C1 is discharged to ground. Hence, the charge in the capacitor C_F will increase for every clock cycle, and hence, the voltage across C_F will also increase with a positive polarity on the terminal of C_F that is connected to the output of the OA. The output of the integrator will now ramp in the positive direction with a step of V_RC_2/C_F for every clock cycle. This condition prevails until the integrator voltage v_{oi} reaches $+V_R$. As soon as $v_{oi} = +V_R$, the comparator output will toggle, and switches S_3, S_4, and S_5 will be changed to position 2. Now, during every clock cycle, the charge in the capacitor C_1 will be transferred to the integrator capacitor C_F, and the charge in C_2 is discharged to ground. Since C_1 is charged from $+V_R$, the charge transferred to the feedback capacitor C_F will now be in the opposite direction compared to the earlier case, and hence, the output voltage of

the integrator will ramp down with a step size of $V_R C_1/C_F$ for every clock. The integrator voltage v_{oi} will ramp down until it reaches $-V_R$. As soon as v_{oi} becomes $-V_R$, the comparator output will toggle again, and switches S_3, S_4 and S_5 will go back to position 1. Now, the circuit will operate as explained initially, thus leading to sustained oscillation.

4.2 Capacitance to pulse-width modulator

The capacitance-to-pulse-width modulator (PWM) circuit is schematically shown in Fig. 15, where, for the sake of simplicity, the sensor C_x is represented without parasitic elements, while C_R and C_I are constant capacitances [16]. The circuit includes three Miller integrators based on the operational transconductance amplifiers (OTAs) INT1, INT2 and INT3, and an OTA with two in-phase matched output ports, indicated by OTA2 in Fig. 15.

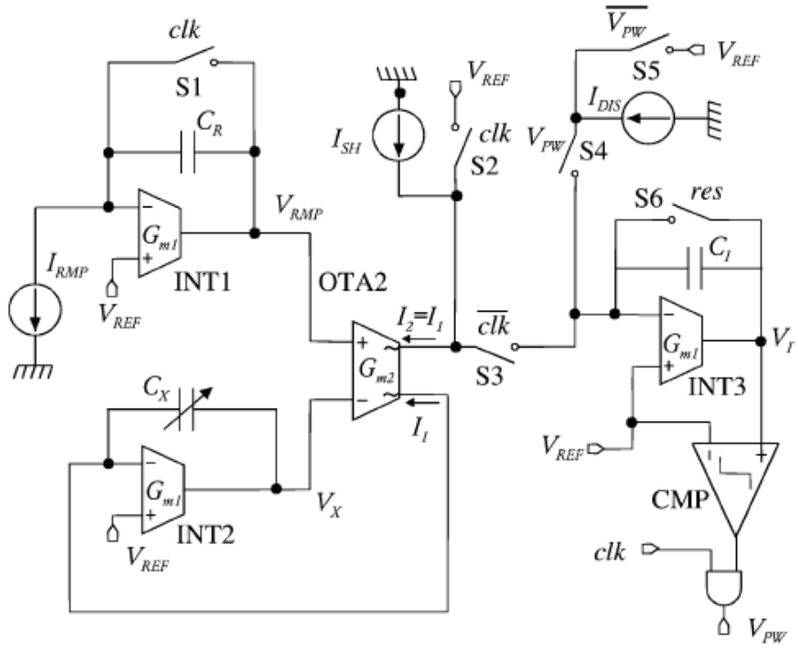

Fig. 15. Simplified schematic view of the capacitance to pulse duration converter [16].

The control signals of switches S1 to S6 are indicated by the labels in the figure. V_{PW} is the output pulse-duration-modulated signal, synchronous to the clock, which, in turn, is a 50% duty-cycle square wave with a period of T_{ck}. In normal operation the res signal is high, so that S_6 is open. INT1 integrates the current during the clock lower level, producing a ramp, and it is discharged to the reference voltage during the clock higher level. V_{REF} works as the zero level for all the three integrators. The integrator INT2 is closed in a feedback loop through OTA2 forcing INT2 output voltage, V_X, to track the INT1 output V_{RMP}. For this reason, the increments of V_X and V_{RMP} across the whole clock lower level are the same, that is,

$$\frac{1}{C_X}=\int_0^{T_{CK}/2} I_1 dt=\frac{1}{C_R}=\int_0^{T_{CK}/2} I_{RMP} dt=\frac{T_{CK} I_{RMP}}{2C_R} \tag{18}$$

Notice that, due to the AND gate, the voltage is forced to be low during the clock lower level, regardless of the comparator (CMP) output. Therefore, the integrator INT3 integrates the difference between the current I_2, which is a replica of I_1, and the constant current I_{SH}

(integration phase). The INT3 initial output voltage (V_I) must be equal to V_{REF}. Setting I_{SH} smaller than the maximum value of I_2, V_I gets higher than V_{REF} during the integration phase and the CMP output turns high. As the clock switches to the high level, INT3 is disconnected from OTA2 by S3, V_{PW} turns high and, consequently, C_I starts to be discharged (de-integration phase) by the constant current I_{DIS}, connected to INT3 by S4. This phase ends when V_{PW} is set low by CMP, i.e., when the INT3 output voltage crosses again the starting voltage V_{REF}. This occurs when the whole charge stored during the integration phase is released. Since INT3 output voltage is held at V_{REF} until the clock is raised again, the value V_{REF} is actually the starting point of the next integration phases, as supposed in the discussion above. The output pulse duration coincides with the duration of the de-integration phase:

$$\int_0^{T_{CK}/2} \left(I_2 - I_{SH}\right) dt = \int_0^{T_{PW}} I_{DIS}\, dt = T_{PW} I_{DIS} \tag{19}$$

Combing (18) and (19) and considering that I_{DIS} is a constant current, we get the expression of the pulse duration:

$$T_{PW} = \frac{T_{Ck}}{2} k_1 \left(\frac{C_X - k_2 C_R}{C_R} \right) \tag{20}$$

where $k_1=I_{RMP}/I_{DIS}$ and $k_2=I_{SH}/I_{RMP}$.

4.3 Capacitance to duty-cycle converter

A capacitance to duty-cycle (CDC) conversion circuit is shown in Fig. 16.

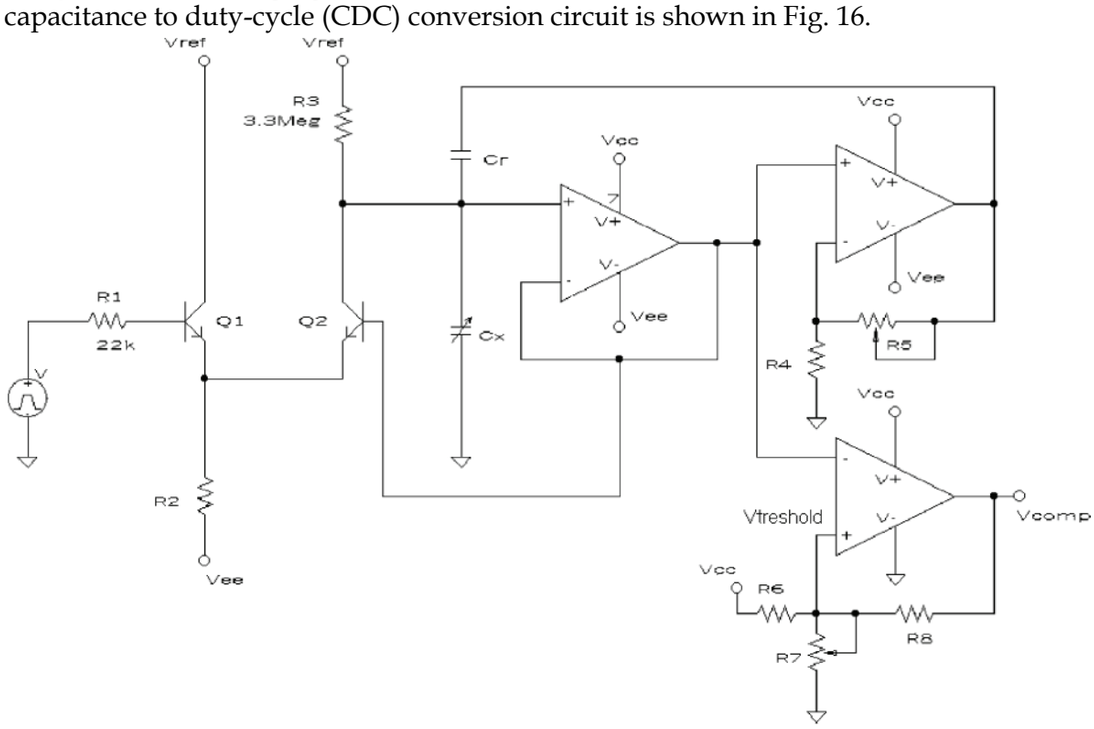

Fig. 16. Capacitance to Duty-Cycle conversion circuit[17].

The CDC converter consists of an RC circuit, a switch, a voltage follower, a feedback amplifier and an output comparator. From the response of an RC circuit, it is well known that the time T at which the voltage across the capacitor reaches a given value $V_{threshhold}$ depends linearly on the capacitance

$$T = RC \ln \frac{V_{CC}}{V_{CC} - V_{threshold}} \tag{21}$$

To achieve as large a bandwidth as possible, feedback has been incorporated in the circuit, as shown in Fig. 17.

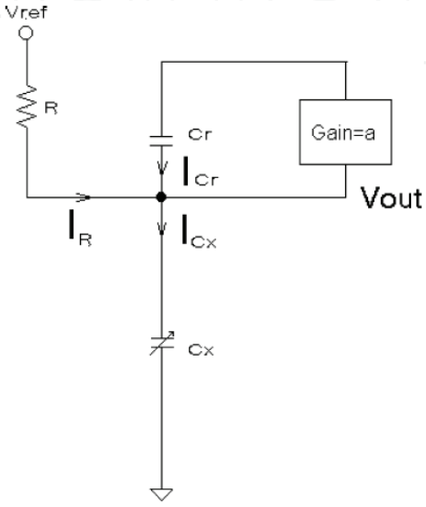

Fig. 17. Feedback loop in the CDC converter.

The feedback path consists on an amplifier and a reference capacitance C_r. For the circuit in Fig. 17, we have:

$$I_R + I_{Cr} = I_{Cx} \tag{22}$$

$$\frac{V_{ref} - V_{out}}{R} + C_r \frac{d}{dt}\left(aV_{out} - V_{out}\right) = C_x \frac{dV_{out}}{dt} \tag{23}$$

From equation 23, it can be shown that:

$$T = R\left[C_x - (a-1)C_r\right] \ln \frac{V_{ref}}{V_{ref} - V_{threshold}} \tag{24}$$

Without feedback, the time T at which the voltage reaches $V_{threshold}$ depends solely on C_x. In this case, the minimum value of CDC (T_{min}) occurs when $C_x=C_{xmin}$, and the maximum value of T (T_{max}) occurs when $C_x=C_{xmax}$. In many capacitive sensing elements, the difference between the maximum and minimum values of C_x is a small fraction of its nominal value (C_{xnom}). Hence, without feedback, the nominal value T_{nom}, would be much larger than the dynamic range of T. Furthermore, the time duration for one CDC conversion must be at least T_{min}; therefore, without feedback, the conversion time will have a redundant baseline T_{nom} value resulting in reduced bandwidth of the CDC. Employing the feedback path

shown, the conversion time depends linearly on the difference between the variable capacitance C_x and the reference capacitance C_r. This significantly decreases the fixed component of the rise time, and leads to a significant increase of the bandwidth.

4.4 Capacitance to frequency converter

The schematic circuit of the first-order relaxation oscillator is shown in Fig. 18, which is the core of the capacitance to frequency converter [18].

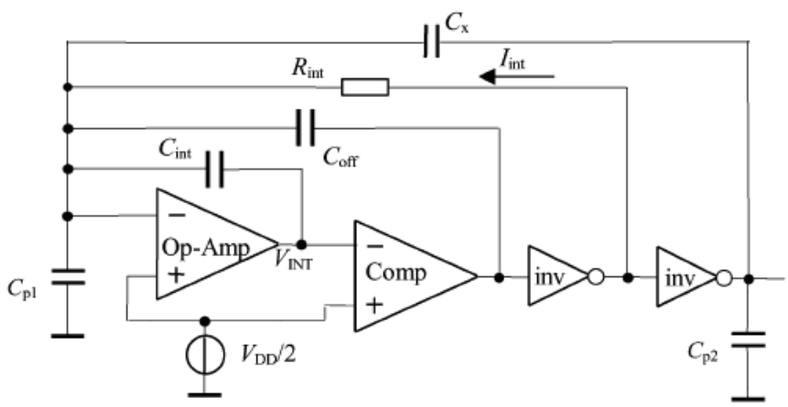

Fig. 18. First-order relaxation oscillator [18].

The oscillator is implemented with an operational amplifier (op-amp), a comparator (comp), two digital inverters, the capacitances C_{off} and C_{int}, and a controlled current source I_{int}, whose value depends on the resistor R_{int}. The capacitor C_x represents the capacitance of the sensor to be measured and C_{p1} and C_{p2} model the parasitic capacitances to ground due to, for example, the connecting cables. When the voltage at the output of the op-amp crosses the threshold level $V_{DD}/2$, the output of the comparator and the inverters switch, and the charge is transferred from capacitors C_x and C_{off} to C_{int}, generating a step voltage at the op-amp output. Next, the current I_{int} removes the charge stored at C_{int} until the op-amp output reaches the threshold level again. The period (T) of the oscillator output signal is given by:

$$T = 4R_{\text{int}}\left(C_{off} + C_x\right). \tag{24}$$

5. Readout electronic circuit for the three dimensional capacitive sensor

The electronic interfaces whose output signals are period, frequency or duty-cycle modulated are the most attractive as their output can be read directly by a digital circuit such as a microcontroller. The main drawback is that the readout speed usually is slow and that, for some architectures, it is capacitance-dependent.

In order to measure the impedance with precision, some care with the parasitics must be taken into account both at the project and at the connection levels. Specifically, the effects of the series and shunt impedances of the wires that connect the sensing elements to the readout electronics have to be taken into account. There are, however, some techniques that reduce these effects.

A good technique to reduce the wire effects consist in the two port measurement. Fig. 19 (a) shows the case of unknown impedance Z_x with series parasitic impedances Z_1 to Z_4. In this

case, the impedances Z_1 to Z_4 do not affect the measurement of the Z_x value: Z_1 and Z_2 are in series with a current source, therefore the current in Z_x is not influenced by them; Z_3 and Z_4 are in series with a voltmeter, therefore their current (and their voltage drop) will be null. Fig. 19 (b) shows the case of the shunt parasitic impedances. The impedances Z_1 and Z_2 do not influence the measurement of Z_x: Z_1 is in parallel with the voltage source V, therefore its current does not influence the measured value; Z_2 is in parallel with the ammeter (which has very low impedance), therefore its current will be null. In a real situation, both the non infinite impedance of the current source and of the voltmeter, for the circuit of Fig. 19 (a), and the non null impedance of the voltage source and of the ammeter, for the circuit of Fig. 19 (b) influence the final result.

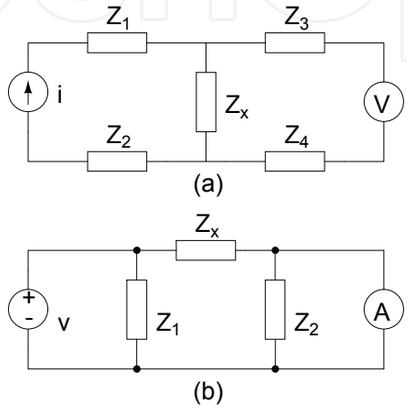

Fig. 19. Two port measurement techniques: (a) with series parasitic impedances; (b) with shunt parasitic impedances.

Based on the two port measurement technique, it is possible to obtain the capacitance value of small capacitors (C_x of Fig. 20) in a precise way, even in the presence of the parasitic capacitances of the wires (C_{P1} and C_{P2}) several orders of magnitude superior than C_x [20, 21].

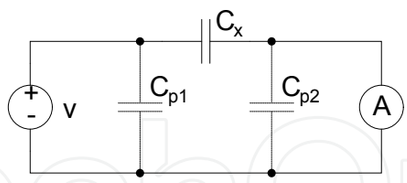

Fig. 20. Two port network for capacitance reading.

In this circuit, the current i measured by the ammeter is given by:

$$i = v\,\omega C \tag{25}$$

where v is the voltage of the source V and $\omega = 2\pi f$. The parasitic capacitances C_{P1} and C_{P2} do not influence the measurement: C_{P1} is in parallel with the voltage source, therefore its current is not measured by the ammeter; C_{P2} is in parallel with the ammeter, i. e., a very low impedance device, therefore its current is close to zero. Notice that the current i measured by the ammeter is directly proportional to the capacitance C of the capacitor, as it is indicated by equation 25. The proportionality constant is $v\omega$.

Fig. 21 shows a block diagram of the capacitance to voltage converter circuit. The voltage source is implemented by an oscillator and the ammeter is implemented by a very low input

impedance current to voltage converter. In order to output a voltage signal proportional to the capacitance, the current to voltage converter must be followed by a full wave rectifier and a low pass filter.

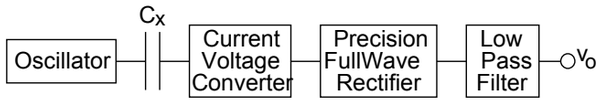

Fig. 21. Block diagram of the circuit.

Fig. 22 shows the schematic diagram of the circuit where the functional blocks of Fig. 21 are implemented by simple configurations.

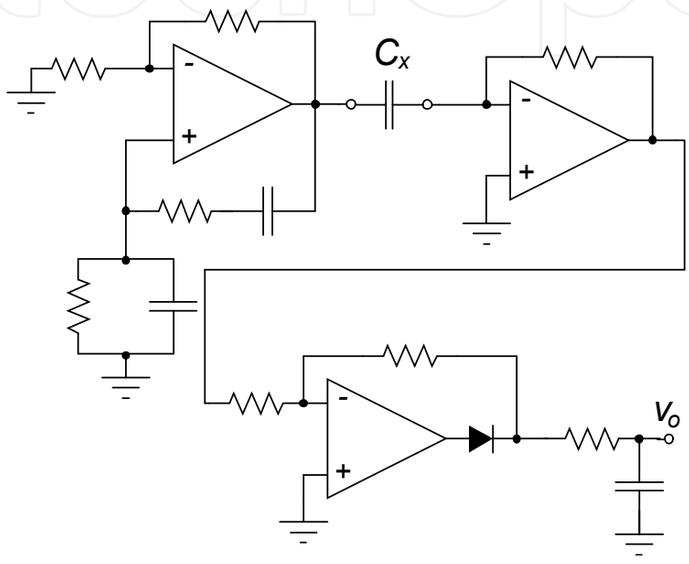

Fig. 22. Schematic diagram of the readout circuit.

6. Conclusions

A three dimensional capacitive force sensor for tactile applications has been presented. In order to better understand its capabilities, the different technologies developed in order to achieve tactile sensors have been reviewed. In this way, electromagnetic, piezoelectric, resistive and piezoresistive based tactile sensors have been discussed. Finally, the three dimensional capacitive force sensor has been presented. In a first stage, the theoretical description of the sensor has been developed through the simulation of the sensor response to forces applied along different directions. Finally, the readout electronics for capacitive sensors in general and for the three dimensional capacitive sensor has been shown.
As a conclusion, capacitive sensors allow an easy and low-cost fabrication of a flexible and precise three-dimensional force sensor suitable for tactile applications.

7. References

I. Bennion, J. A. R. Williams, L. Ahang, K. Sugden, and N. J. Doran; "UV-written in-fibre Bragg gratings," Opt. Quantum Electron., Vol. 28, 1996, pp. 93-135.

B. M. Cowie, D. J. Webb, B. Tam, P. Slack and P. N. Brett, "Fibre Bragg grating sensors for distributive tactile sensing," Meas. Sci. Technol., vol. 18, 2007, pp. 138-146.

J. S. Heo, J. H. Chung, J. J. Lee, "Tactile sensor arrays using fiber Bragg grating sensors," Sensors and Actuators A, vol. 126, 2006, pp. 312-327.
Y. Tanaka, M. Tanakaand S. Chonan, "Development of a sensor system for collecting tactile information," Microsyst Technol, vol. 13, 2007, pp. 1005-1013.
T. Hemsel, R. Stroop, D. Oliva Uribe, J. Wallaschek, "Resonant vibrating sensors for tactile tissue differentiation," Journal of Sound and Vibration, vol. 308, 2007, pp. 441-446.
K. Motoo, F. Arai and T. Fukuda, "Piezoelectric Vibration-Type Tactile Sensor Using Elasticity and Viscosity Change of Structure" IEEE Sensors Journal, Vol. 7, 2007, pp.1044-1051.
E. S. Hwang, J. Seo and Y. J. Kim, "A Polymer-Based Flexible Tactile Sensor for Both Normal and Shear Load Detections and Its Application for Robotics," Journal of Microelectromechanical Systems, Vol. 16, 2007, pp. 556-563.
M. Ádám, T. Mohácsy, P. Jónás, C. Dücso, E. Vázsonyi, I. Bársony, "CMOS integrated tactile sensor array by porous Si bulk micromachining," Sensors and Actuators A 142, 2008, 192-195.
M. Balke, E. Peiner and L. Doering, "A new micromachined sensor system for tactile measurements of high aspect ratio microstructures," Microsyst Technol Vol. 14, 2008, pp. 543-549.
A. Wisitsoraat, V. Patthanasetakul, T. Lomas, A. Tuantranont, "Low cost thin film based piezoresistive MEMS tactile sensor," Sensors and Actuators A 139, 2007, 17-22.
R. Matsuzaki and A. Todoroki; "Wireless flexible capacitive sensor based on ultra-flexible epoxy resin for strain measurement of automobile tires," Sensors and Actuators A 140 (2007) 32–42.
C. Metzgera, E. Fleisch, J. Meyer, M. Dansachmüller, I. Graz, M. Kaltenbrunner, C. Keplinger, R. Schwödiauer and Siegfried Bauerb; "Flexible-foam-based capacitive sensor arrays for object detection at low cost," Applied Physics Letters 92, 013506 2008.
W. Bracke, P. Merken, R. Puers, C. Van Hoof; "Design methods and algorithms for configurable capacitive sensor interfaces," Sensors and Actuators A 125 (2005) 25–33.
B. George and V. J. Kumar, "Switched Capacitor Signal Conditioning for Differential Capacitive Sensors," IEEE Transactions on Instrumentation and Measurement, Vol. 56, No. 3, 2007 pp. 913-917.
P. Bruschi, D. Navarrini, G. Barillaro and A. Gola; "A Precise Capacitance-to-Pulse Width Converter for Integrated Sensors," Analog Integrated Circuits and Signal Processing, 42, 2005, 185–189.
P. Bruschi, N. Nizza, and M. Piotto, "A Current-Mode, Dual Slope, Integrated Capacitance-to-Pulse Duration Converter," IEEE J. of Solid-State Circuits, Vol. 42, 2007, pp. 1884-1891.
Z. Ignjatovic, and M. F. Bocko; "An Interface Circuit for Measuring Capacitance Changes Based Upon Capacitance-to-Duty Cycle (CDC) Converter," IEEE Sensors Journal, Vol. 5, No. 3, June 2005, 403-410.
M. Gasulla, X. Li and G. C. M. Meijer; "The Noise Performance of a High-Speed Capacitive-Sensor Interface Based on a Relaxation Oscillator and a Fast Counter," IEEE Transactions on Instrumentation and Measurement, Vol. 54, No. 5, October 2005, 1934-1940.
A. S. Hou and S. X. Su; "Design of a capacitive-sensor signal processing system with high accuracy and short conversion time," Sensors and Actuators A 119 (2005) 113–119.
A. Srivastava, "Digital CMOS interface circuit for current and capacitance sensing," Proceedings of SPIE, Vol. 5389, 2004, pp. 1-12.
F. M. van der Goes and G. C. Meijer, "A universal transducer interface for capacitive and resistive sensor elements," Analog Integrated Circuits and Signal Processing, 14, 1997, pp. 249-260.

Sensors: Focus on Tactile Force and Stress Sensors

Edited by Jose Gerardo Rocha and Senentxu Lanceros-Mendez

ISBN 978-953-7619-31-2
Hard cover, 444 pages
Publisher InTech
Published online 01, December, 2008
Published in print edition December, 2008

This book describes some devices that are commonly identified as tactile or force sensors. This is achieved with different degrees of detail, in a unique and actual resource, through the description of different approaches to this type of sensors. Understanding the design and the working principles of the sensors described here requires a multidisciplinary background of electrical engineering, mechanical engineering, physics, biology, etc. An attempt has been made to place side by side the most pertinent information in order to reach a more productive reading not only for professionals dedicated to the design of tactile sensors, but also for all other sensor users, as for example, in the field of robotics. The latest technologies presented in this book are more focused on information readout and processing: as new materials, micro and sub-micro sensors are available, wireless transmission and processing of the sensorial information, as well as some innovative methodologies for obtaining and interpreting tactile information are also strongly evolving.

How to reference

In order to correctly reference this scholarly work, feel free to copy and paste the following:

Jose Gerardo Rocha and Senentxu Lanceros-Mendez (2008). Three Dimensional Capacitive Force Sensor for Tactile Applications, Sensors: Focus on Tactile Force and Stress Sensors, Jose Gerardo Rocha and Senentxu Lanceros-Mendez (Ed.), ISBN: 978-953-7619-31-2, InTech, Available from: http://www.intechopen.com/books/sensors-focus-on-tactile-force-and-stress-sensors/three_dimensional_capacitive_force_sensor_for_tactile_applications

INTECH
open science | open minds

InTech Europe
University Campus STeP Ri
Slavka Krautzeka 83/A
51000 Rijeka, Croatia
Phone: +385 (51) 770 447
Fax: +385 (51) 686 166
www.intechopen.com

InTech China
Unit 405, Office Block, Hotel Equatorial Shanghai
No.65, Yan An Road (West), Shanghai, 200040, China
中国上海市延安西路65号上海国际贵都大饭店办公楼405单元
Phone: +86-21-62489820
Fax: +86-21-62489821

IntechOpen